Electronic Supplementary Material (ESI) for Journal of Materials Chemistry C.


## Electronic Supporting Information

# A 3D metal–organic framework built by vanadate clusters and diamond chains showing weak ferromagnetic single-chain-magnet like behavior

Rong Li,[a,b] Yu Xiao,[c] Shuai-Hua Wang,[a,*] Xiao-Ming Jiang,[a] Ying-Ying Tang,[a] Jian-Gang Xu,[a,b] Yong Yan,[a,b] Fa-Kun Zheng,[a,*] and Guo-Cong Guo[a]

[a] *State Key Laboratory of Structural Chemistry, Fujian Institute of Research on the Structure of Matter, Chinese Academy of Sciences, Fuzhou, Fujian 350002, P. R. China*

[b] *University of Chinese Academy of Sciences, Beijing 100039, P. R. China*

[c] *School of Pharmaceutical Science, Harbin Medical University, Harbin 150086, P. R. China*

### Materials and instruments

All chemicals were commercially available sources of analytical grade and used without further purification. The elemental analysis was performed on an Elementar Vario EL III microanalyzer. The FT-IR spectra were obtained on a Perkin-Elmer Spectrum using KBr disks in the range 4000–400 $cm^{-1}$. $^1H$ NMR (400 MHz) spectra were recorded on a Bruker AVANCE 400 NMR spectrometer with $Me_4Si$ as the internal standard in deuterated solvent DMSO-$d_6$.Thermogravimetric analysis (TGA) experiment was made on a NETZSCH STA 449C Jupiter thermogravimetric analyzer under air atmosphere with the sample heated in an $Al_2O_3$ crucible at a heating rate of 10 K $min^{-1}$. Powdered *X*-ray diffraction data (PXRD) were collected on a Miniflex II diffractometer using Cu-*K*α radiation ($\lambda$ = 1.540598 Å) at 40 kV and 40 mA in the range of $5° \leq 2\theta \leq 60°$. The simulated patterns were derived from the Mercury Version 1.4 software (*http://www.ccdc.cam.ac.uk/products/mercury/*). Magnetic data were collected on a Quantum Design MPMS-XL SQUID magnetometer using crushed samples (in the powdered form).

**Caution!** Sodium azide and tetrazolate compounds are energetic materials, which might explode under certain conditions. So it needs to take care during the preparation and handling

of the compounds, which should be used only a small quantities.

**Synthesis of (cmb)Cl and 1.**

**(cmb)Cl**: A mixture of chloroacetonitrile (2.27 g, 0.03 mol) and 4,4'-bipyridine (4.68 g, 0.03 mol) in 25 mL DMF was stirred for 2 h, and then heated to 80 °C. The stirring was continued and kept to this temperature for 1 day, and then the brown precipitates were filtered. The compound *N*-(cyanomethyl)-4,4′-bipyridinium chloride ((cmb)Cl) was obtained with 53% yield. NMR analysis for (cmb)Cl, $^1$H NMR (400 MHz, $D_2O$): δ 9.20 (d, $J$ = 6.3 Hz, 2H), 8.88 (d, $J$ = 6.5 Hz, 2H), 8.57 (d, $J$ = 6.8 Hz, 2H), 8.41 (d, $J$ = 6.7, 2H), 5.52 (d, $J$ = 6.1 Hz, 2H). Anal. Calcd for $C_{12}H_{10}N_3Cl$: C, 62.21; H, 4.35; N, 18.14 %. Found: C, 62.93; H, 4.61; N, 18.56%.

**$[Co_3(N_3)_2(V_4O_{12})(tzmb)_2(H_2O)_3]\cdot 5H_2O$ (1)**: The reaction mixture of (cmb)Cl (0.139g, 0.6 mmol), $CoCl_2\cdot 6H_2O$ (0.214g, 0.9 mmol) , $NH_4VO_3$ (0.140g, 1.2 mmol) and $NaN_3$ (0.098g, 1.5 mmol) in 8.0 mL of distilled water was sealed into a 25 mL teflon-lined stainless steel vessel under autogenous pressure and then heated to 140 °C in 2 hours and kept to this temperature for 2 days and cooled to room temperature at a rate of 5 °C/h. Sheet crystals of **1** for suitable for X-ray analysis were obtained. Yield: 37% (based on Co). Anal. Calcd for $C_{24}H_{36}N_{18}O_{20}V_4Co_3$: C, 22.57; H, 2.84; N, 19.74%. Found: C, 22.32; H, 2.76; N, 19.85%. The experimental PXRD pattern of the bulk products is consistent with the calculated one based on the single-crystal data, indicating pure phase of **1** (Fig. S13). Thermogravimetric analyses (TGA) curves (Fig. S14) show that a weight loss up to 180 °C occurred in **1**, and then the breakdown of the framework took place when temperature rose higher than 240 °C.

**Crystal Structure Determination**

Single crystal of **1** was mounted on glass fibers. The single-crystal X-ray diffraction measurement was performed on a Rigaku Saturn-724 CCD for **1** which was equipped with a graphite-monochromatic Mo-$K_\alpha$ radiation source ($\lambda$ = 0.71073 Å) by the $\omega$ scan mode. The structure was solved by the direct methods using the SHELXTL version 5 package.[1] Subsequent successive differences Fourier syntheses yielded other non-hydrogen atoms. The final structure was refined using a full-matrix least-squares refinement on $F^2$. All non-

hydrogen atoms were refined anisotropically. Hydrogen atoms of ligands were added geometrically and refined using the riding model. Hydrogen atoms of all water molecules were located in the idealized positions and refined with O–H distances restrained to a target value of 0.85 Å, the H···H distance to 1.34 Å, and $U_{iso}$(H) = 1.5 $U_{eq}$(O). All of the calculations were performed by the Siemens SHELXTL version 2014/6 package of crystallographic software.[2] Pertinent crystal data and structural refinement results, and selected bond distances and angles for **1** are listed in Tables S1 and S2, respectively.

**References**

[1] CrystalClear, version 1.35, Software User's Guide for the Rigaku R–Axis, and Mercury and Jupiter CCD Automated X–ray Imaging System, Rigaku Molecular Structure Corporation, Utah, 2002.

[2] Sheldrick, G. M. *Acta Cryst.* **2015**, *C71*, 3–8.

**Table S1.** Crystal data and structure refinement parameters for **1.**

| Compound | **1** |
|---|---|
| Formula | $C_{24}H_{34}N_{18}O_{20}V_4Co_3$ |
| Formula mass | 1277.26 |
| Space group | *P*–1 |
| *a*/Å | 9.3497(17) |
| *b*/Å | 12.145(3) |
| *c*/Å | 20.743(5) |
| $\alpha$/° | 88.020(13) |
| $\beta$/° | 82.993(13) |
| $\gamma$/° | 68.326(7) |
| *V*/Å$^3$ | 2172.4(8) |
| Z | 2 |
| $D_c$ /g cm$^{-3}$ | 1.953 |
| $\mu$/mm$^{-1}$ | 2.037 |
| *F*(000) | 1274 |
| reflns collected | 17993 |
| unique reflns | 8025 |
| $R_{int}$ | 0.0347 |
| GOF | 1.013 |
| $R_1$ [a][$I > 2\sigma(I)$] | 0.0514 |
| $wR_2$[b] (all data) | 0.1318 |
| *CCDC No.* | 993176 |

[a]$R_1 = \Sigma||F_o| - |F_c||/\Sigma|F_o|$, [b]$wR_2 = \Sigma[(w(F_o^2 - F_c^2)^2)/\Sigma[w(F_o^2)^2)]^{1/2}$

**Table S2.** Bond lengths (Å) and angles (deg) of **1**.

| | | | |
|---|---|---|---|
| Co(1)–O(1) | 2.020(3) | Co(3)–O(11)#4 | 2.016(3) |
| Co(1)–N(17) | 2.103(4) | Co(3)–N(14)#5 | 2.153(4) |
| Co(1)–N(16)#1 | 2.152(4) | Co(3)–O(2W) | 2.170(4) |
| Co(1)–N(7) | 2.154(4) | Co(3)–N(4) | 2.174(4) |
| Co(1)–N(2) | 2.158(4) | Co(3)–O(1W) | 2.224(4) |
| Co(1)–N(11) | 2.201(4) | V(1)–O(3) | 1.594(4) |
| Co(2)–O(7) | 2.024(3) | V(1)–O(1) | 1.664(3) |
| Co(2)–N(17) | 2.095(4) | V(1)–O(2) | 1.771(4) |
| Co(2)–N(6)#2 | 2.161(4) | V(1)–O(4) | 1.807(3) |
| Co(2)–N(12) | 2.162(4) | V(2)–O(6) | 1.628(4) |
| Co(2)–O(3W) | 2.169(4) | V(2)–O(5) | 1.665(3) |
| Co(2)–N(1) | 2.199(4) | V(2)–O(2)#3 | 1.762(4) |
| Co(3)–O(5)#3 | 2.007(3) | V(2)–O(4) | 1.800(3) |
| V(4)–O(12) | 1.628(4) | V(3)–O(9) | 1.610(4) |
| V(4)–O(11) | 1.654(3) | V(3)–O(7) | 1.664(3) |
| V(4)–O(8)#6 | 1.761(3) | V(3)–O(8) | 1.759(3) |
| V(4)–O(10) | 1.810(3) | V(3)–O(10) | 1.814(3) |
| | | | |
| O(1)–Co(1)–N(17) | 176.94(15) | O(1)–Co(1)–N(11) | 96.83(14) |
| O(1)–Co(1)–N(16)#1 | 89.17(14) | N(17)–Co(1)–N(11) | 84.20(14) |
| N(17)–Co(1)–N(16)#1 | 93.67(15) | N(16)#1–Co(1)–N(11) | 92.64(14) |
| O(1)–Co(1)–N(7) | 92.16(14) | N(7)–Co(1)–N(11) | 170.98(14) |
| N(17)–Co(1)–N(7) | 86.85(15) | N(2)–Co(1)–N(11) | 86.09(14) |
| N(16)#1–Co(1)–N(7) | 86.82(16) | O(7)–Co(2)–N(17) | 174.71(15) |
| O(1)–Co(1)–N(2) | 95.23(14) | O(7)–Co(2)–N(6)#2 | 90.68(14) |
| N(17)–Co(1)–N(2) | 81.95(15) | N(17)–Co(2)–N(6)#2 | 91.86(14) |
| N(16)#1–Co(1)–N(2) | 175.54(14) | O(7)–Co(2)–N(12) | 94.70(13) |
| N(7)–Co(1)–N(2) | 93.76(15) | N(17)–Co(2)–N(12) | 82.66(14) |
| N(6)#2–Co(2)–N(12) | 174.41(15) | O(5)#3–Co(3)–O(11)#4 | 168.09(14) |
| O(7)–Co(2)–O(3W) | 90.66(14) | O(5)#3–Co(3)–N(14)#5 | 93.91(14) |
| N(17)–Co(2)–O(3W) | 84.86(15) | O(11)#4–Co(3)–N(14)#5 | 94.50(14) |
| N(6)#2–Co(2)–O(3W) | 86.47(14) | O(5)#3–Co(3)–O(2W) | 87.58(14) |
| N(12)–Co(2)–O(3W) | 91.96(14) | O(11)#4–Co(3)–O(2W) | 83.80(14) |
| O(7)–Co(2)–N(1) | 100.03(14) | N(14)#5–Co(3)–O(2W) | 177.86(15) |
| N(17)–Co(2)–N(1) | 84.46(14) | O(5)#3–Co(3)–N(4) | 93.48(13) |
| N(6)#2–Co(2)–N(1) | 93.29(14) | O(11)#4–Co(3)–N(4) | 94.16(14) |
| N(12)–Co(2)–N(1) | 87.27(14) | N(14)#5–Co(3)–N(4) | 95.08(14) |
| O(3W)–Co(2)–N(1) | 169.30(14) | O(2W)–Co(3)–N(4) | 86.36(15) |
| O(5)#3–Co(3)–O(1W) | 83.79(14) | N(14)#5–Co(3)–O(1W) | 84.50(15) |
| O(11)#4–Co(3)–O(1W) | 88.64(14) | O(2W)–Co(3)–O(1W) | 94.14(16) |

Symmetry codes for **1**: #1 *–x*, *–y*, *–z*; #2 *–x* + 2, *–y*, *–z* – 1; #3 *–x* + 1, *–y* + 1, *–z*; #4 *–x* + 1, *–y* + 1, *–z* – 1; #5 *x* + 1, *y*, *z*; #6 *–x*, *–y* + 1, *–z* – 1; #7 *x* – 1, *y*, *z*.

**Scheme S1.** From the experimental results we can see that the intrachain magnetic interactions are crucial at low temperatures and field induced metamagnetic transitions. Five magnetic exchange parameters are considered, including intrachained $J_1$, $J_2$, $J_3$, $J_4$ and $J_5$, in which $J_1$ is the strongest coupling between the nearest neighboring spin sites $Co^{2+}$ within the magnetic chains. The coupling $J_2$, $J_3$, $J_4$ and $J_5$ within the chains were also included in the calculation to cover the possible minor but important interactions. The 1D Ising-like diamond-chain is simplified as following mode:

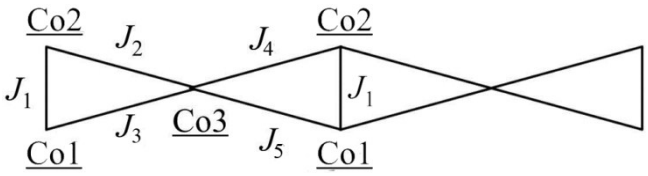


Spin-polarized *DFT* calculations employed the projector augmented wave method encoded in the Vienna ab initio simulation package, the local density approximation (*LDA*), and the plane wave cutoff energy of 500 eV.[3,4] The *LDA* plus on-site repulsion *U* method *LDA* + *U* was employed to properly describe the electron correlation associated with Co 3d states ($U$ (0) = 3 eV). Finally, we can get magnetic exchange parameters: $J_1$ = –0.24 emV, $J_2$ = 0.01 emV, $J_3$ = 0.01 emV, $J_4$ = 0.04 emV and $J_5$ = 0.03 emV. The large negative value of $J_1$ suggests strong antiferromagnetic interactions between Co1 and Co2. The positive sign of $J_2$–$J_5$ indicates the weak ferromagnetic interactions between Co3 and Co1 (or Co2) in the diamond chain. The energy expressions of the nine ordered spin states ($S$= 3/2 for $Co^{2+}$) can be expressed as:[5]

$$E\,(FM) = E_0 + 2S^2(J_1 + J_2 + J_3 + J_4 + J_5)$$

$$E\,(AF1) = E_0 + 2S^2(J_2 + J_4)$$

$$E\,(AF2) = E_0 + 2S^2(J_3 + J_5)$$

$$E\,(AF3) = E_0 + 2S^2J_1$$

$$E\,(AF4) = E_0 + 2S^2(J_3 - J_5)$$

$$E\,(AF5) = E_0 + 2S^2(J_2 - J_4)$$

$$E\,(AF6) = E_0 + 2S^2(-J_1 - J_3 - J_5 + J_2 + J_4)$$

$$E\,(AF7) = E_0 + 2S^2(-J_1 - J_2 - J_4 + J_3 + J_5)$$

$$E\,(AF8) = E_0 + 2S^2(J_1 - J_2 - J_4 - J_3 - J_5)$$

**References**

[3] H. J. Xiang, E. J. Kan, Su-Huai Wei, M.-H. Whangbo, and X. G. Gong, *Phys. Rev. B*, 2011, **84**, 224429.

[4] H. Xiang, C. Lee, H.-J. Koo, X. Gong and M.-H. Whangbo, *Dalton Trans.*, 2013, **42**, 823.

[5] X.-M. Jiang, X.-G. Li, M.-J. Zhang, Z.-F. Liu, Y. Liu, J.-M. Liu and G.-C. Guo, *Sci. Rep.*, 2015, **5**, 17344.

**Table S3.** The values of magnetic exchange parameters $J_1$–$J_5$.

| | $J_1$ | $J_2$ | $J_3$ | $J_4$ | $J_5$ |
|---|---|---|---|---|---|
| Distance/Å | 3.496 | 6.122 | 6.496 | 6.538 | 6.168 |
| Value/emV | –0.24 | 0.01 | 0.01 | 0.04 | 0.03 |

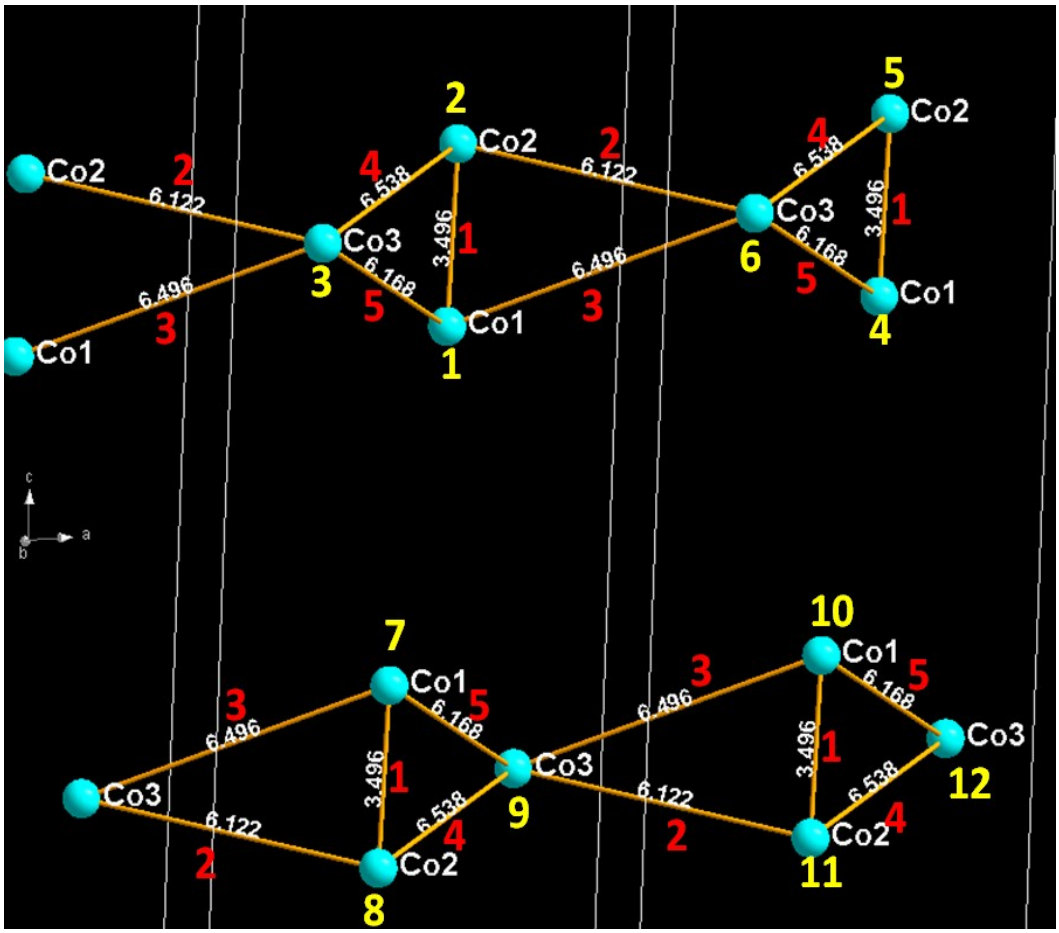

**Scheme S2.** At a fixed temperature, the in-phase ($\chi'$) and the out-of-phase ($\chi''$) components of the *ac* magnetic susceptibility were measured as the frequency ($\omega$) of the *ac* field (dc = 0 Oe amplitude) varied from 0.1 to 689.3 Hz. These data were best fit to a distribution of single relaxation processes, following the expressions for $\chi'(\omega)$ and $\chi''(\omega)$:

$$\chi'(\omega) = \chi_S + \frac{(\chi_T - \chi_S)[1 + (\omega\tau)^{1-\alpha}sin\frac{\alpha\pi}{2}]}{1 + 2(\omega\tau)^{1-\alpha}sin\frac{\alpha\pi}{2} + (\omega\tau)^{2(1-\alpha)}}$$

$$\chi''(\omega) = \frac{(\chi_T - \chi_S)(\omega\tau)^{1-\alpha}cos\frac{\alpha\pi}{2}}{1 + 2(\omega\tau)^{1-\alpha}sin\frac{\alpha\pi}{2} + (\omega\tau)^{2(1-\alpha)}}$$

In these equations, $\chi_s = \chi_{W\to\infty}$ is the adiabatic susceptibility, $\chi_s = \chi_{T\to\infty}$ is the isothermal susceptibility, $\omega = 2\pi\nu$ is the angular frequency, and $\tau$ is the magnetization relaxation time.

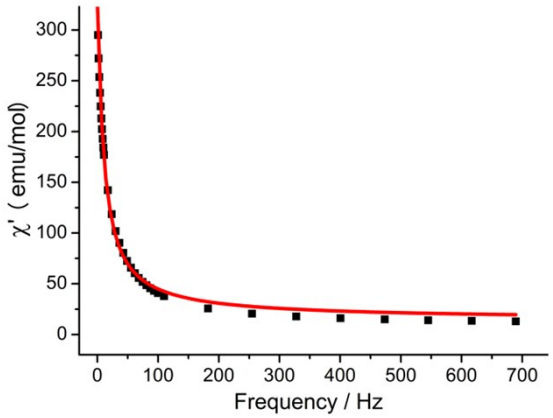


$\chi'$ vs frequency for **1** at 3.5 K was illustrated in the figure above, and the data are fit to a distribution of single relaxation processes, as described the equation. This gives the parameters of $\chi_T$ = 12.90 emu/mol, $\chi_T$ = 330.4 emu/mol, $\tau$ = 0.0141 s and $\alpha$ = 0.2635.

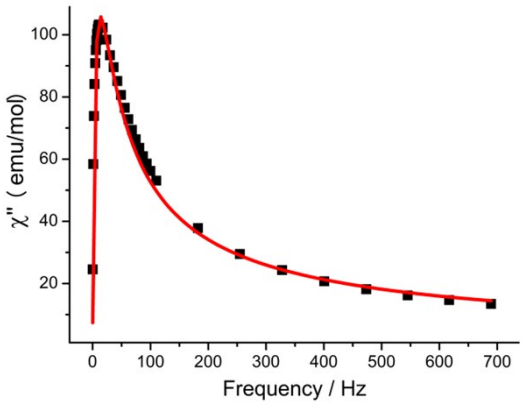


The data of $\chi''$ vs frequency are fit to a distribution of single relaxation processes and gives the parameters of $\tau$ = 0.0121 s and $\alpha$ = 0.2511. The resulting relaxation times from these two fitting data are very similar.

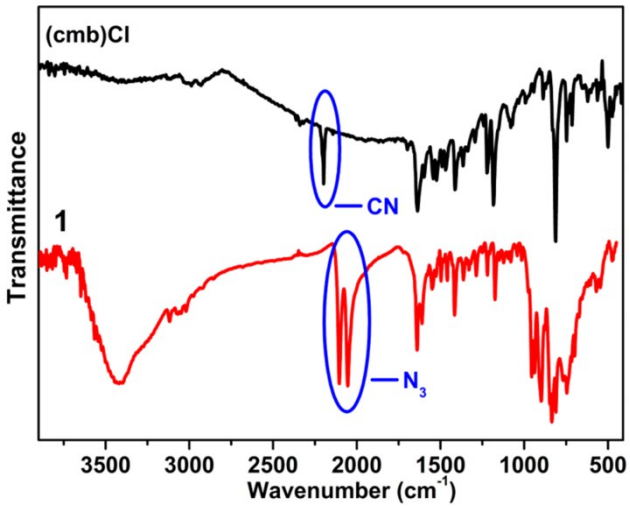


**Fig. S1** IR spectrum of (cmb)Cl and **1**.

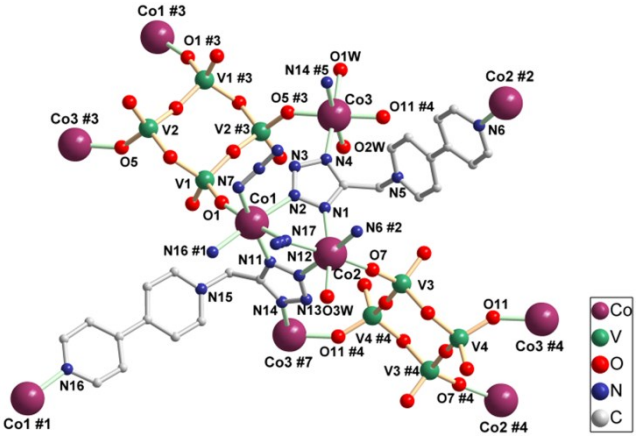


**Fig. S2** The coordination and linkage modes of metals and ligands in **1**, with H atoms omitted for clarity. Symmetry codes: #1 –*x*, –*y*, –*z*; #2 2 – *x*, –*y*, –1 – *z*; #3 1 – *x*, 1 – *y*, –*z*; #4 1 – *x*, 1 – *y*, –1 – *z*; #5 1 + *x*, *y*, *z*; #7 –1 + *x*, *y*, *z*.

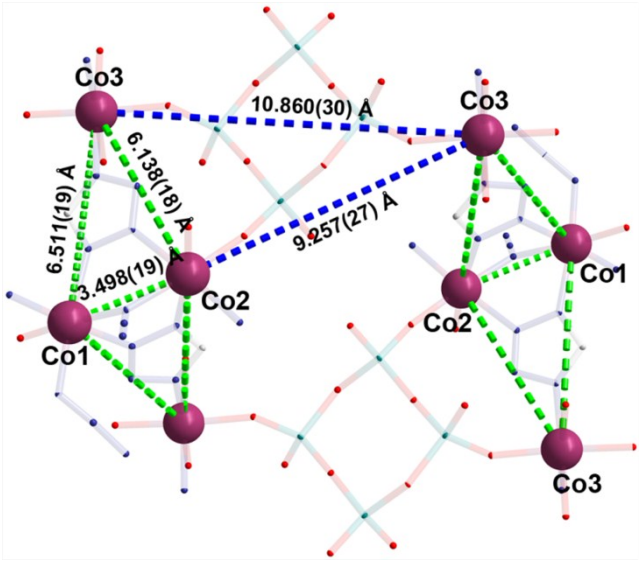


**Fig. S3** View of the Co···Co distances linked by the tetrazole ligand and the shortest interchain exchange pathway (as a yellow arrow) through the diamagnetic $[V_4O_{12}]^{4-}$ ligand in **1**.

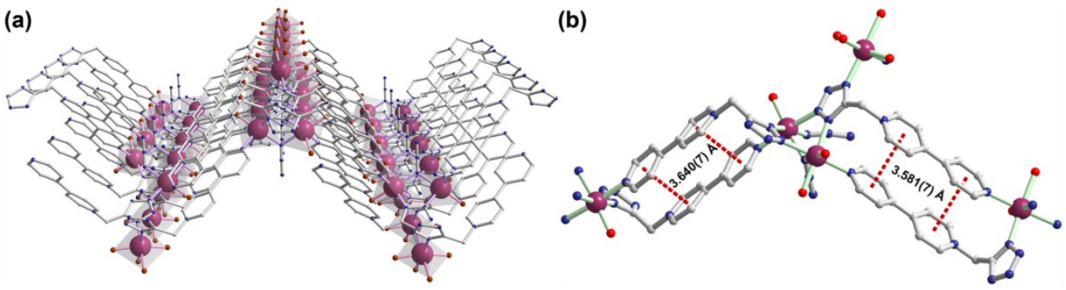


**Fig. S4** (a) Perspective view of the metal-organic layer in **1**; (b) The face-to-face π–π interactions with the center-to-center distances of 3.6408(7) Å and 3.5817(7) Å in the framework of **1**.

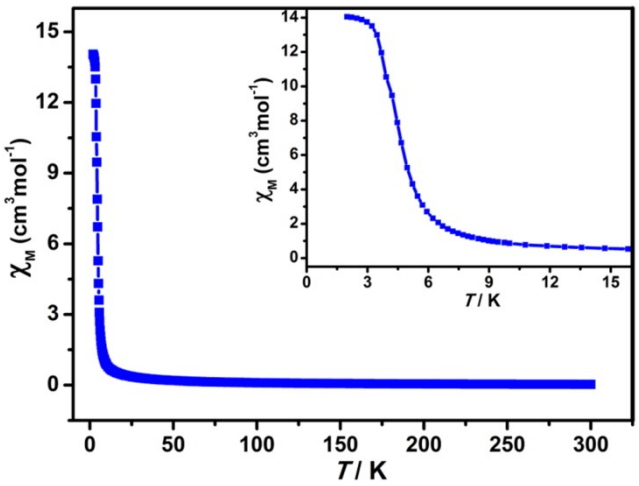


**Fig. S5.** $\chi_M$ vs $T$ plot for **1** at applied fields of 1 kOe.

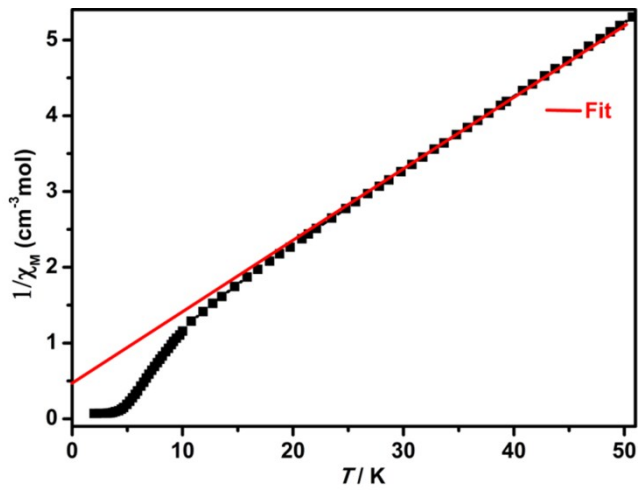


**Fig. S6** The plot of $1/\chi_M$ *vs.* $T$ at 1 kOe.

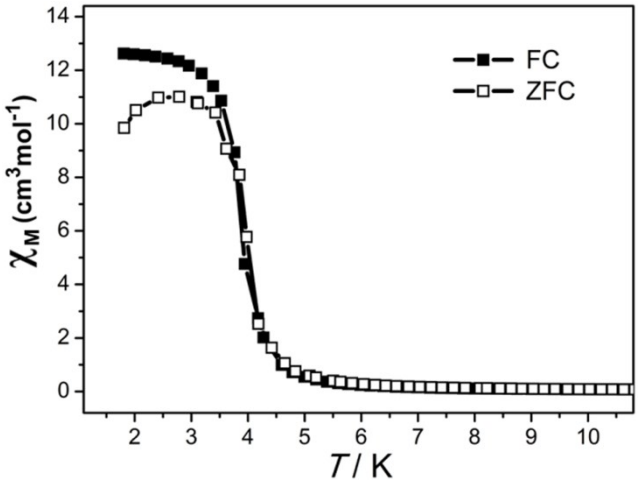


**Fig. S7** FC and ZFC curves of **1** measured in the magnetic field of 1 kOe.

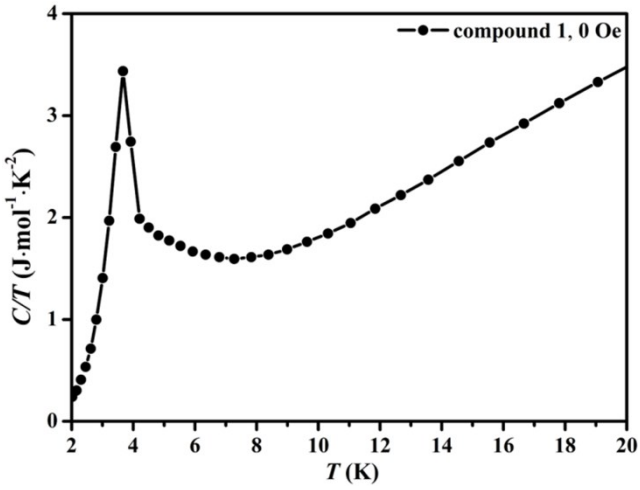


**Fig. S8** Heat capacity of **1** measured at zero magnetic field.

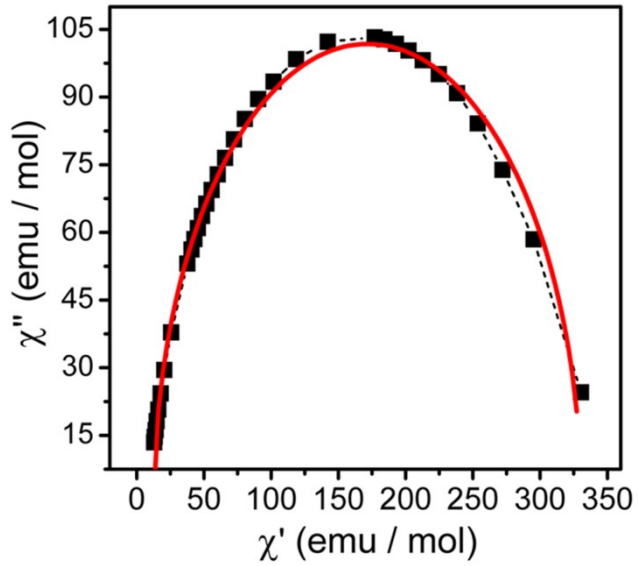


**Fig. S9** Cole-Cole diagram at 3.5 K for **1** ($H_{ac}$ = 3 Oe, $H_{dc}$ = 0 Oe); The red solid line represents the least-squares fit using a Debye model.

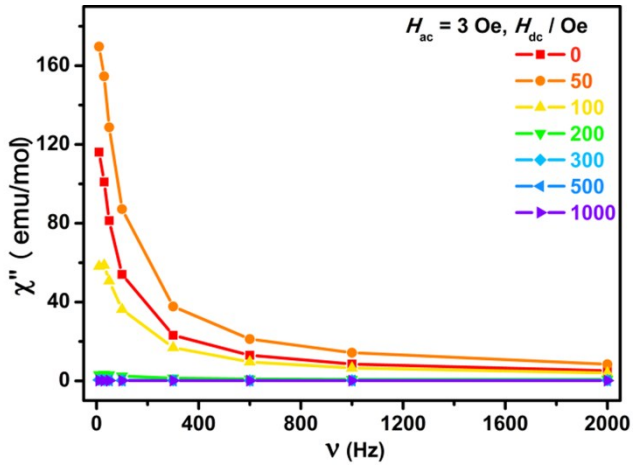


**Fig. S10** $\chi$" vs frequency for **1** under various *dc* fields at 3.5 K.

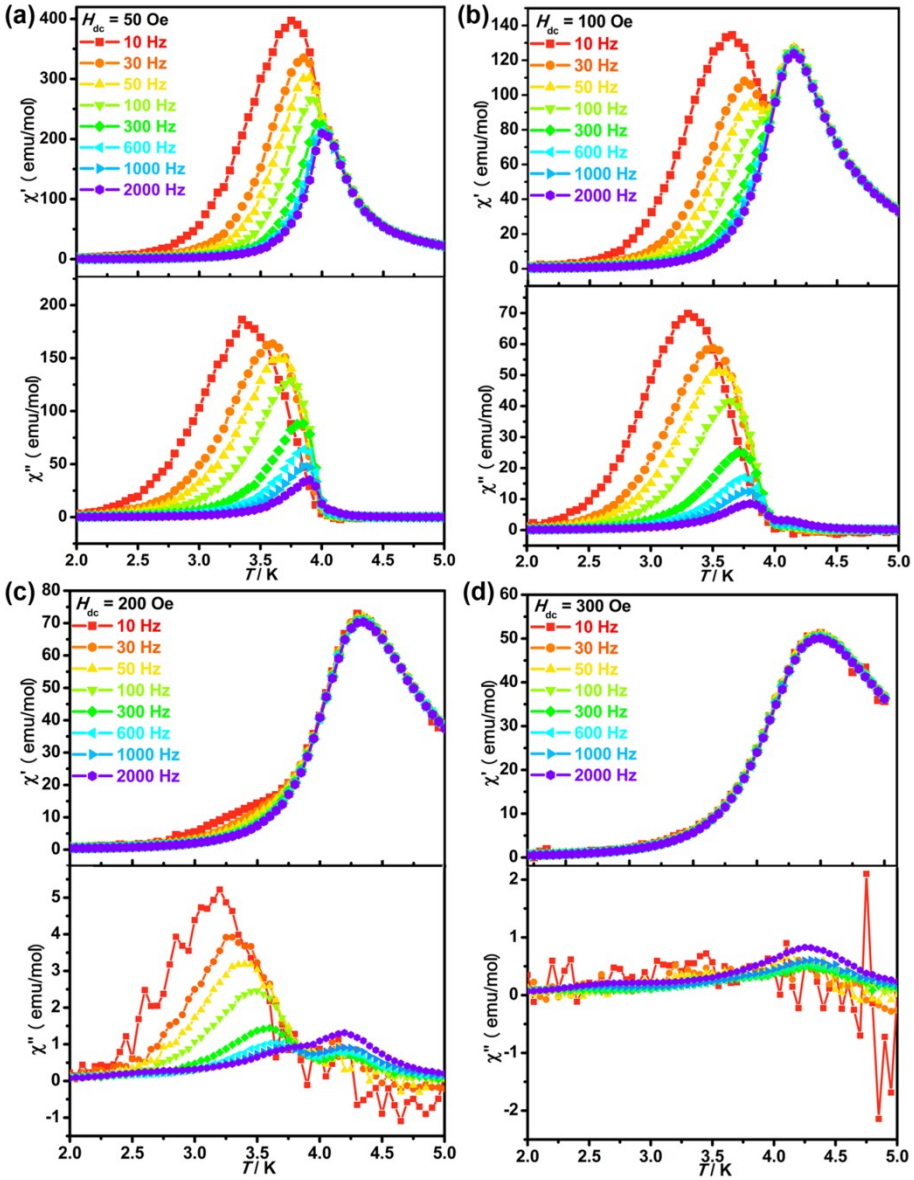


**Fig. S11** The *ac* plots for **1** between 2 and 5 K at different frequencies with $H_{ac}$ = 3.0 Oe, $H_{dc}$ = 50, 100, 200 and 300 Oe, respectively.

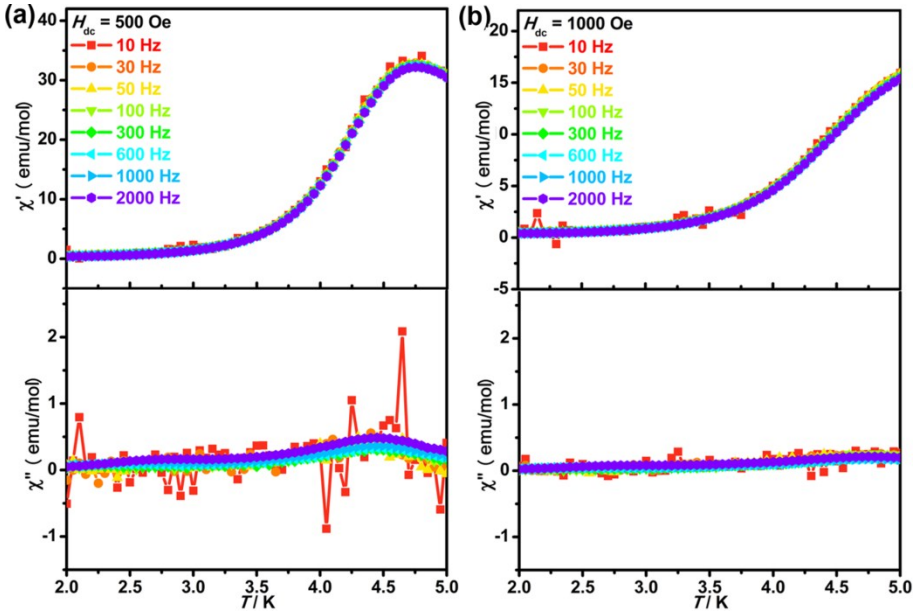


**Fig. S12** The *ac* plots for **1** between 2 and 5 K at different frequencies with $H_{ac}$ = 3.0 Oe, $H_{dc}$ = 500 and 1000 Oe respectively.

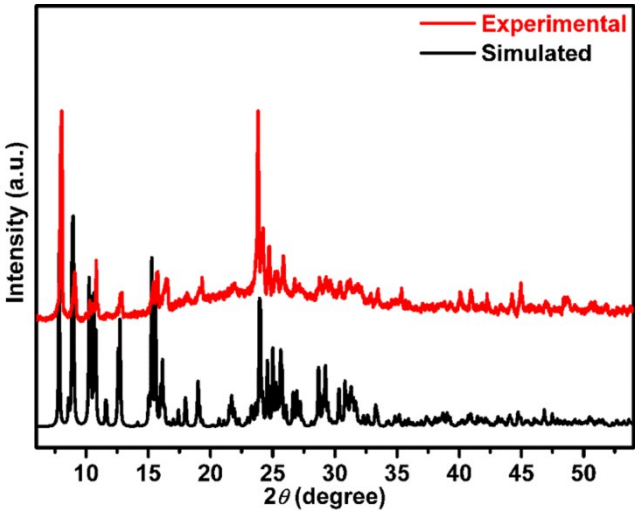


**Fig. S13** Powered *X*-ray diffraction (PXRD) pattern of **1**.

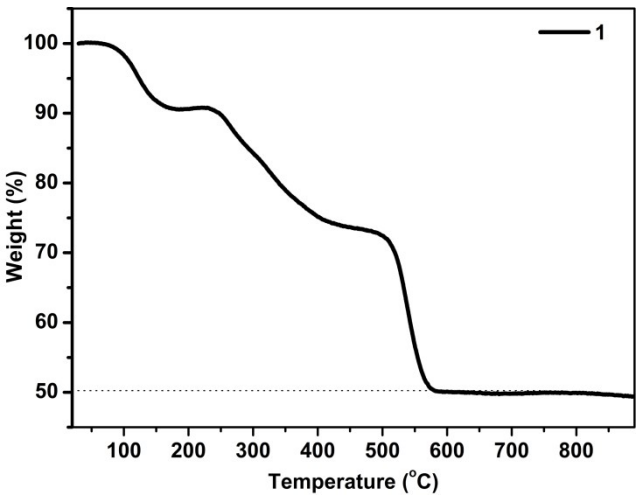


**Fig. S14** The TGA curve for **1**.